IEEE Access
Multidisciplinary | Rapid Review | Open Access Journal

Received December 2, 2019, accepted January 1, 2020, date of current version January 16, 2020.

Digital Object Identifier 10.1109/ACCESS.2020.2964271

Deep Residual Haze Network for Image Dehazing and Deraining

CHUANSHENG WANG[1,2], ZUOYONG LI[1,3], JIAWEI WU[1], HAOYI FAN[2], GUOBAO XIAO[1], AND HONG ZHANG[2]

[1]Fujian Provincial Key Laboratory of Information Processing and Intelligent Control, Minjiang University, Fuzhou 350121, China
[2]School of Computer Science and Technology, Harbin University of Science and Technology, Harbin 150080, China
[3]The Fujian College's Research Base of Humanities and Social Science for Internet Innovation Research Center, Minjiang University, Fuzhou 350121, China

Corresponding authors: Zuoyong Li (fzulzytdq@126.com) and Hong Zhang (zhangh@hrbust.edu.cn)

This work was supported in part by the National Natural Science Foundation of China under Grant 61972187 and Grant 61702101, in part by the Natural Science Foundation of Fujian Province under Grant 2017J01768 and Grant 2019J01756, in part by the Key Project of College Youth Natural Science Foundation of Fujian Province under Grant JZ160467, in part by the Fujian Provincial Leading Project under Grant 2017H0030 and Grant 2019H0025, in part by the Government Guiding Regional Science and Technology Development under Grant 2019L3009, and in part by the Technology Project of Education Department of Fujian Province under Grant JT180406.

ABSTRACT Image dehazing on a hazy image aims to remove the haze and make the image scene clear, which attracts more and more research interests in recent years. Most existing image dehazing methods use a classic atmospheric scattering model and natural image priors to remove the image haze. In this paper, we propose an end-to-end image dehazing model termed as DRHNet (Deep Residual Haze Network), which restores the haze-free image by subtracting the learned negative residual map from the hazy image. Specifically, DRHNet proposes a context-aware feature extraction module to aggregate the contextual information effectively. Furthermore, it proposes a novel nonlinear activation function termed as RPReLU (Reverse Parametric Rectified Linear Unit) to improve its representation ability and to accelerate its convergence. Extensive experiments demonstrate that DRHNet outperforms state-of-the-art methods both quantitatively and qualitatively. In addition, experiments on image deraining task show that DRHNet can also serve for image deraining.

INDEX TERMS Image dehazing, image deraining, negative residual map, context-aware feature extraction, reverse parametric rectified linear unit (RPReLU).

I. INTRODUCTION

The goal of the image dehazing algorithm is to restore a hazy image to a clear image, which has received significant research interest because various advanced image processing tasks require a clear scene (e.g., [1]–[6]). Traditional image dehazing algorithms (e.g., [7], [8]) are dedicated to accurately estimate the transmission and the global atmospheric light in hazy images, and then use the atmospheric scattering model to restore haze-free images. McCartney [9] first proposed the atmospheric scattering model, which is further developed by Narasimhan and Naya [10], [11]. The atmospheric scattering model can be formally written as:

$$I(x) = J(x)t(x) + \alpha(1 - t(x)) \tag{1}$$

where $I(x)$ is the haze-degraded image, $J(x)$ is the haze-free scene, α is the global atmospheric light, and $t(x)$ is the scene transmission that describes the portion of the light that is not scattered and reaches the camera sensors. In practice, $t(x)$ and α are not provided in advance. Therefore, most prior based image dehazing algorithms attempt to estimate $t(x)$ and α and then recover the haze-free scene using Eq. (1).

The estimation of $t(x)$ plays a significant role that directly impacts the performance of haze removal algorithms. However, these transmission approximations are often inaccurate, especially in the scenes where the color of an object is inherently similar to the haze [7], [8]. Therefore, the traditional image dehazing algorithms are not robust enough to handle images in some special conditions. So, there are numerous defects when adopting traditional algorithms to perform image dehazing task. With the prosperous advancement of deep learning, an increasing number of researchers have explored image dehazing algorithms using convolution

The associate editor coordinating the review of this manuscript and approving it for publication was Gang Li.

This work is licensed under a Creative Commons Attribution 4.0 License. For more information, see http://creativecommons.org/licenses/by/4.0/

(a) Hazy image (b) Our dehazing result (c) Rain image (d) Our deraining result

FIGURE 1. The results of the proposed DRHNet for image dehazing and deraining.

neural networks (CNNs) [12]–[15]. Among them, [12] and [15] adopted a CNN to precisely estimate the transmission $t(x)$. Although these algorithms based on CNNs can estimate the $t(x)$ more accurately, it still needs to estimate the α accurately to recover the haze-free image perfectly.

To overcome the problem mentioned above, we propose a Deep Residual Haze Network (DRHNet) that does not require the estimation of $t(x)$ and α. The primary purpose of DRHNet is to learn the residual between the haze-free image and the hazy image, rather than learning the haze-free image directly. The benefits of this approach are as follows. First, He *et al.* demonstrated in [16] that optimizing the residual mapping is more straightforward than optimizing the original mapping. In the image dehazing task, the residuals between the haze-free image and the hazy image can be thought of as the residual mapping. Second, the complexity of the residual is much lower than the of the haze-free image, so the deep learning network is easier to fit the residual. Third, since the proposed DRHNet is not need the atmospheric scattering model for image dehazing, it can not only process image dehazing task, but also be used for other image enhancement tasks. Fourth, the residual can accurately determine the extent of different regions of the image affected by the haze. Fig. 1 shows the image dehazing and deraining performance of the proposed DRHNet.

Fig. 2 can show the fourth advantage mentioned above. From left to right in Fig. 2, the original hazy image (Fig. 2(a)), the output of the proposed DRHNet (Fig. 2(b)) and the dehazed result (Fig. 2(c)). As far as we know, the haze is evenly distributed in the atmospheric, but the damage degree is not also evenly distribute on each patch. Fig. 2(b) can be used to express the degree of image damage by haze in different areas. For example, as can be seen in the region marked by the white rectangle in Fig. 2, there are little differences between Fig. 2(a) and Fig. 2(c), so the color in the corresponding area pixel in Fig. 2(b) is darker than other region. Therefore, it can be seen from Fig. 2 that the proposed DRHNet not only accurately indicates the effect of the image dehazing algorithm, but also shows the degree of distortion caused by haze in different regions of the same hazy image.

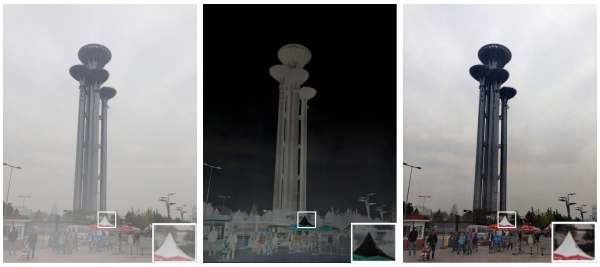

(a) Hazy image (b) Negative residual map (c) Dehazing result

FIGURE 2. From left to right, the original hazy image, the negative residual map obtained from DRHNet and the final dehazed result.

To prove that the proposed DRHNet is useful in the image dehazing task, we conducted a lot of experiments on the RESIDE [17]. The experiment demonstrates that the proposed DRHNet surpasses other leading dehazing algorithms both in quantitative evaluation and qualitative evaluation. Furthermore, additional experiments for image deraining task demonstrate the capability of the generality of the DRHNet. In addition, we also applied DRHNet to other challenging tasks related to image dehazing but not absolutely the same to prove the generality of the proposed DRHNet. A large number of experiments have demonstrated that the proposed DRHNet can not only perfectly handle any image dehazing task, but also show excellent performance in other tasks related to image dehazing. The contributions of this paper are as follows:

- We propose a novel end-to-end image dehazing network called the DRHNet to restore the haze-free image by subtracting the estimated negative residual map from the hazy image. The negative residual map can reflect the extent of haze damage and the dehazing effect explicitly.
- Moreover, a novel activation function, called the reverse parametric rectified linear unit (RPReLU), is designed to improve the representation ability of the dehazing model and accelerate the convergence of the training.
- We conduct extensive experiments on multiple real-world datasets, and the results demonstrate DRHNet's effectiveness compared to other state-of-the-art baselines.

- We also apply the proposed DRHNet for image deraining task, and the results show that DRHNet outperforms the other state-of-the-art image deraining methods, which demonstrates the generalizability of the proposed method.

The remainder of the paper is organized as follows. First, we review the related research in the field of image dehazing in Section II, which provides background knowledge of understanding the DRHNet's design, and then introduce the DRHNet detailedly in Section III. Finally, we conduct the DRHNet with comprehensive experiments results and ablation analysis in Section IV, before the conclusions are given in Section V.

II. RELATED WORK

As the importance of the image dehazing algorithms in the field of computer vision, a lot of image dehazing algorithms have been proposed to solve this challenging problem. These algorithms can be roughly divided into traditional prior-based algorithms and modern learning-based algorithms. The key difference between prior-based algorithms and learning-based algorithms is that the prior-based algorithms extract features through handcrafted approaches, while learning-based algorithms extract features automatically by CNNs. These two completely different ideas have their advantages and defects. In this section, we briefly review some representative image dehazing algorithms that contain both prior-based algorithms and modern learning-based algorithms and discuss their superiorities and disadvantages.

A. ATMOSPHERIC SCATTERING MODEL

Eq. (1) is proposed to describe the formation of a hazy image, which can be rewritten as:

$$J(x) = \frac{I(x) - \alpha(1 - t(x))}{t(x)} \tag{2}$$

where, $t(x)$, α and $J(x)$ are unknowns. According to Eq. (2), the real scene $J(x)$ can be recovered easily after $t(x)$ and α have been estimated. Eq. (2) suggests that α and $t(x)$ are the keys to atmospheric scattering model based image dehazing algorithms. Therefore, most traditional atmospheric scattering model based image dehazing algorithms are dedicated to estimating the transmission $t(x)$ and the global atmospheric light α accurately. In general, with the deepening of scene depth, the more seriously the image is affected by haze, which leads to the decrease of the transmittance. Therefore, the scene transmission $t(x)$ is closely related to the scene depth, which can be expressed as:

$$t(x) = e^{-\beta d(x)} \tag{3}$$

where β is the scattering coefficient of the atmosphere and $d(x)$ is the scene depth. Eq. (3) indicates that if we can estimate the $d(x)$ of the image, then we can use Eq. (3) to estimate $t(x)$, and vice versa.

B. PRIOR-BASED ALGORITHMS

Image prior knowledge is the empirical statistics from the observations of the images. Due to the superiority of the prior-based dehazing algorithms, some important prior-based dehazing algorithms have been proposed [7], [8], [18]–[23]. The two most representative algorithms are the dark channel prior (DCP) [7] (proposed by He *et al.*) and the color attenuation prior (CAP) [8] (proposed by Zhu *et al.*). We introduce these two important image dehazing algorithms in detail.

1) DARK CHANNEL PRIOR

Dark Channel Prior (DCP) is a representative algorithm in the field of image dehazing [7]. He *et al.* made statistics on a large number of haze-free images and found a rule: In most of the nonsky patches of RGB images, at least one color channel has some pixels with very low intensity and close to zero. Equivalently, the minimum intensity in this path is also very low and close to zero. For an arbitrary RGB image J, the dark channel is given by:

$$J^{dark}(x) = min_{y\in\Omega(x)}(min_{c\in\{r,g,b\}}J^c(y)) \tag{4}$$

where, c represents one of the three RGB channels, $\Omega(x)$ is a small patch center on x. A dark channel has two minimum operators: $min_{y\in\{r,g,b\}}$ is the minimum filtering operation of three channels at a pixel, and $min_{y\in\Omega(x)}$ is the minimum filtering operation for the patch centered on x.

2) COLOR ATTENUATION PRIOR

Zhu *et al.* proposed Color Attenuation Prior (CAP) to describe the relevant image features in hazy weather [8]. Zhu *et al.* found that the brightness and the saturation of the hazy images are affected by the haze concentration. To be precise, in a less-affected area with a hazy image, the saturation is pretty high, and the brightness is within the normal range. However, if a certain region of the image is seriously affected by haze, its brightness will rise sharply, but its saturation will decline. As a result, the difference between the brightness and saturation becomes larger. As the haze concentration increases with the depth of the scene in general, Zhu *et al.* deduced that:

$$d(x) \propto c(x) \propto v(x) - s(x) \tag{5}$$

where, the $d(x)$ is the scene depth, $c(x)$ is the haze concentration, the $c(x)$ and $v(x)$ is the saturation and the brightness respectively. Therefore, the depth of the image with hazy can be approximately estimated by the Color Attenuation Prior (CAP), so the transmittance of the scene can be estimated by Eq. (3).

C. LEARNING-BASED ALGORITHMS

Although the DCP and CAP are effective estimators of haze concentration, there are still some defects, such as their inability to accurately estimate the atmospheric light α and adaptively adjust the parameters. The problems associated with these two algorithms also appear in other prior-based approaches.

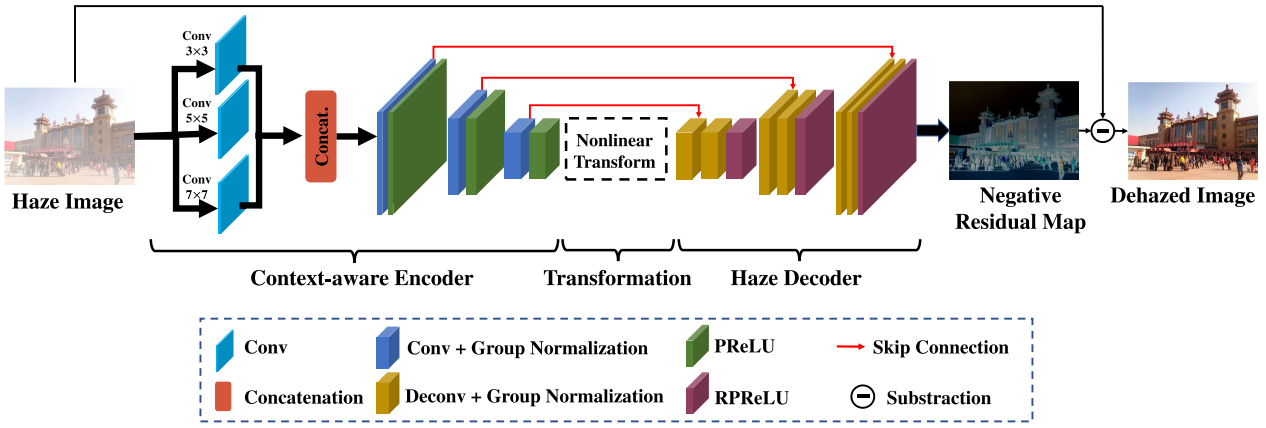

FIGURE 3. The framework of the proposed DRHNet.

In recent years, researchers have progressively focused on utilizing CNNs to estimate the transmission of the hazy image and use Eq. (2) to restore the haze-free image [12], [14]. But it is not completely out of the bounds of the traditional image dehazing algorithm, which causes the disadvantages of the traditional image dehazing algorithm also exist in these learning-based algorithms. For example, it is necessary to estimate the $t(x)$ and α to recover the haze-free image from the hazy image perfectly. Different from these image dehazing algorithms that combine deep learning and atmospheric scattering model, the proposed DRHNet is to learn the residual between the network's output (clear image) and input (hazy image), which significantly reduces the complexity of the image dehazing task. Therefore, the proposed DRHNet can achieve an excellent effect on image dehazing task.

III. THE PROPOSED DRHNeT

As illustrated in Fig. 3, the proposed DRHNet consists of three components, the context-aware encoder (left side), transformation (middle), and haze decoder (right side). The DRHNet learns the residuals between the clear images and hazy images directly because reformulating the layers as learning residual functions is useful to decrease computational burden [16]. In the image dehazing task, clear images are the layer outputs, while hazy images are the layer inputs. Therefore, the DRHNet is directly motivated to learn the residual between the clear image and the hazy image. The dehazed result generated by DRHNet can be generated as follow:

$$J = DRHNet(I) + I \tag{6}$$

where J is the dehazed result, $DRHNet(I)$ is the output of the proposed DRHNet, I is the hazy image. Since the proposed DRHNet generates the residual between clear image and hazy image directly, rather than $t(x)$ and α, Eq. (2) can not be used to restore the haze-free image.

We propose a context-aware feature extraction module to aggregate contextual information and then encode it into the feature maps. Subsequently, we adopt a transformation module to extract the high-level feature. These feature maps will be decoded back by the haze decoder to estimate the residual map. Because the residual between haze and the haze-free image is negative in most of the region, we put the negative residual map obtained by taking the opposite value of each pixel of the residual map obtained from DRHNet in Fig. 3 to provide convenience for readers to understand this concept. Finally, the haze-free image is obtained by subtracting the hazy image to the negative residual. It's worth note that we put a Group Normalization layer (GN) [24] after each convolutional layer because GN is stable in a wide range of batch sizes and its computational cost is independent of batch sizes. In Section IV, we will show GN is more suitable than Batch Normalization (BN) [25], Instance Normalization (IN) [26], and Layer Normalization (LN) [27] for the image dehazing task. The following subsections will introduce the detailed design of the proposed DRHNet.

A. DESIGN OF THE CONTEXT-AWARE ENCODER

The context-aware feature extraction module has been proposed to make DRHNet extract features effectively. In this section, we detail the context-aware feature extraction module and how to use it in the context-aware encoder component.

1) CONTEXT-AWARE FEATURE EXTRACTION MODULE

The most significant characteristic of hazy image is that different regions of the hazy image are affected by different degrees of haze, but the influence degree of each pixel affected by haze is very close to its surrounding areas. Therefore, it is necessary to use multi-scale convolution to extract the features of hazy image. To aggregate the contextual information, the kernel sizes of the context-aware encoder component are set to 3, 5, and 7, respectively, and the dimensions of the feature maps obtained from each part of context-aware encoder component are 64, 32, and 32 respectively, these feature maps are concatenated together. The formula to calculate the size of the feature maps are as follows:

$$W' = (W - F + 2P)/S + 1 \tag{7}$$

$$H' = (H - F + 2P)/S + 1 \tag{8}$$

where W' and H' are the widths and the heights of the output feature map, respectively, F is the kernel size, S represents for stride, P is the number of surrounding layers filled in the feature map. According to Eq. (7) and Eq. (8), we can use P to ensure the equality of the output sizes of the feature maps obtained by different F.

2) CONTEXT-AWARE ENCODER COMPONENT

Image dehazing is an important image processing task that has high requirements on the integrity of the spatial image information [7]. In the first layer of the proposed DRHNet, we adopt the context-aware feature extraction module to aggregate the contextual information. The next layer is obtained from the previous layer by the convolution with a kernel size of 3 and a step size of 2. There are only three-layer convolutions in the context-aware encoder component. The size of the feature map of the next convolution is half of the size of the feature graph of the previous convolution. Generally, the pixel value of haze-free images is lower than that of the hazy images, but sometimes the opposite happens. Therefore, parametric rectified linear unit (PReLU) is used in this context-aware encoder component, because PReLU improves model fitting with nearly zero extra computational cost and keeps the areas of the negative axis [28]. The function of PReLU is shown in Fig. 5(a).

B. TRANSFORMATION COMPONENT

The depth of CNN has a significant influence on the dehazing networks' performance. He *et al.* provides a large number of experiments to prove that the strategy of adopting bottleneck building blocks to extract features is easier to optimize deep networks [16]. To improve the performance of the DRHNet, the bottleneck building blocks [16] are used in the transformation component to learning residual functions with reference to the layer inputs, instead of learning unreferenced functions. In the experiment part, we will explore the best trade-off between the performance and the number of parameters.

1) REVERSE PARAMETRIC RECTIFIED LINEAR UNIT

Choosing the correct activation function is essential for image dehazing algorithms. We design a useful activation function inspired by some traditional haze removal algorithms. References [7] and [8] proved that the pixel values of hazy images are higher than the haze-free image. The DCP [7] demonstrated that the pixel values of the dark channel increase after the image is affected by haze, and the CAP [8] showed that the brightness of the image would increase after being affected by the haze. Therefore, the residual obtained from DRHNet should be a negative matrix. Based on this prior knowledges, we maintain the original signal strength in the negative part of the activation function and suppress the original signal by adding coefficients in the positive part. This activation function (denoted as RPReLU) is shown in Fig. 5(b) and can be written as:

$$RPReLU(x) = \begin{cases} ax_i, & if\ x > 0 \\ x_i, & otherwise \end{cases} \tag{9}$$

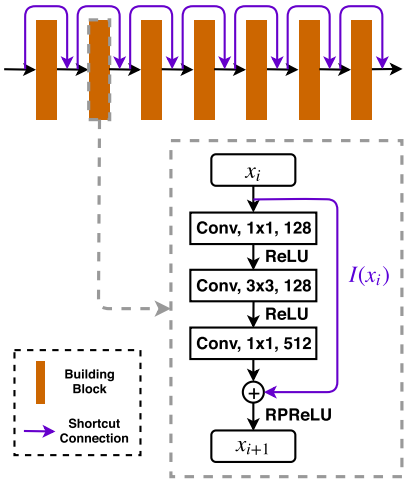

FIGURE 4. The architecture of the proposed transformation component.

where the coefficient a is set to 0.1, and i represents the different channels. RPReLU is useful to the proposed DRHNet and the effectiveness has been validated in the experimental section.

2) DESIGN OF TRANSFORMATION COMPONENT

The relationship between the hazy image and the residual is nonlinear. Therefore, the transformation component converts the hazy information into high-dimensional residual information. As illustrated in Fig. 4, the structure of the transformation component is composed of seven bottleneck building blocks [16]. Different from traditional CNNs, a bottleneck building block performs a mapping as follows:

$$x_{i+1} = RPReLU(F(x_i, w_i) + I(x_i)) \tag{10}$$

where x_i and x_{i+1} are the input and output of the ith bottleneck building block, respectively, w_i is a set of weights and biases associated with ith block and $I(.)$ is the identify function. To obtain a superior tradeoff between the runtime and the performance, we set the dimension of the bottleneck block to 512.

C. HAZE DECODER COMPONENT

The motivation of the DRHNet is to learn the residual between the haze-free image and the hazy image accurately. It is necessary to concatenate the features obtained by the haze decoder component with features obtained by haze decoder component because the features extracted from the shallow module of DRHNet is significant for the dehazing performance. RPReLU is also used in the haze decoder component because the primary purpose of haze decoder is to estimate the residual map from high-level features obtained from the transformation component. Because the structure of the proposed DRHNet is symmetric, the other parameters of the haze decoder component are set the same as the context-aware encoder component. Finally, the haze decoder component outputs the residual between hazy and haze-free image

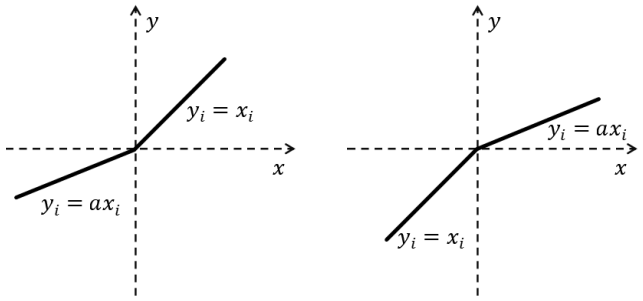

(a) PReLU (b) RPReLU

FIGURE 5. Parametric Rectified Linear Unit (PReLU) [28] and the proposed Reverse Parametric Rectified Linear Unit (RPReLU).

and uses the residual map and the original input hazy image to obtain the dehazed image by Eq. (6).

D. LOSS FUNCTION

1) MEAN SQUARE ERROR

A lot of data-driven dehazing networks use the mean square error (MSE) as a loss function [12], [29]. However, unlike previous works, our goal is to learn the residuals between the hazy scenes and clear scenes. To clearly describe the aforementioned target, let $I_n = \{(I_n), n = 1, \ldots, N\}$ denote the hazy image data set, where $G_n = \{(G_n), n = 1, \ldots, N\}$ is the corresponding ground truth clear image for I_n. In the sequel, we omit the subscript n since inputs are all independent of one another. Therefore, the residual between the ground truth and the hazy image can be described as follows:

$$R = G - I \tag{11}$$

where G is the ground truth image, I is the hazy image. So, the first part of the loss function is described as:

$$L = \|DRHNet(I) - R\|^2 \tag{12}$$

where, $DRHNet(I)$ is the residual obtained by DRHNet.

2) FEATURE RECONSTRUCTION LOSS

We use the feature reconstruction loss [30] as the second part of the loss function. Li *et al.* have proved that the similar images are similar both in their underlying and high-level features extracted from the complex deep learning model named as the "loss network [30]." Therefore, we run images through the loss network to extract features and measure the similarities between their underlying and high-level features. We chose the VGG-16 model [31] as our loss network and used the first, second, and third layers as the measurement to determine the loss function. The formula is as follows:

$$L_p = \sum_{i=1}^{3} \frac{1}{C_i H_i W_i} \|VGG_i(R) - VGG_i(DRHNet(I))\|_2^2 \tag{13}$$

where, $VGG()$ is the network of VGG-16 model, R is the residual between the ground truth and the hazy image. H, W, and C represents the length, width, and the number of channels of the feature map, i represents the number of layers of the VGG-16.

The final loss function can be described as follow:

$$L_{total} = L + \gamma L_p \tag{14}$$

where γ is set to 0.5 in this paper, it is noted that designing the loss function is not our primary focus, but the proposed DRHNet also can achieve state-of-the-art performance in image dehazing task.

IV. EXPERIMENTS

In this section, we conduct sufficient experiments to verify the superiority of the proposed DRHNet. By default, the network is trained for 120 epochs. The default initial learning rate is 0.1 and decays by 0.01 every 40 epochs. All experiments are performed on a server with an Intel(R) Xeon(R) CPU E5-2620, 128GB RAM, and NVIDIA TITAN X. More results and the code can be found at https://github.com/fpklipic/DRHNet.

A. DATASETS

We adopt the benchmark datasets to train and test the proposed DRHNet. To ensure the fairness of the comparison experiment, we use the same training and testing datasets for each comparison algorithms.

1) IMAGE DEHAZING DATASET

For the image dehazing algorithms, most algorithms only use their datasets for evaluation, which makes it is difficult for researchers to compare the proposed algorithms with these algorithms. Therefore, Li *et al.* proposed a benchmark dataset (named RESIDE) to compare different dehazing algorithms [17]. To ensure the fairness of the comparison experiment, we adopt the same training strategy to train the proposed DRHNet and other comparison algorithms in RESIDE. In addition, we also collect 30 real-world hazy images for evaluating to demonstrate the superiority of the proposed DRHNet in the real hazy scene.

2) IMAGE DERAINING DATASET

The field of image deraining also has public datasets for training and testing the image deraining algorithms. Recently, Zhang *et al.* proposed a useful dataset [36] to train and test the state-of-the-art image deraining networks, which contains raining density tags of light rain, moderate rain, and heavy rain. We ignore these tags and use the whole training set to train the proposed DRHNet. Although ignoring the raining density tags degrades the performance, the DRHNet still surpasses the previous state-of-the-art image deraining algorithms.

B. QUANTITATIVE AND QUALITATIVE EVALUATION FOR IMAGE DEHAZING TASK

The quantitative and qualitative evaluations on the synthetic dataset and real-world hazy images are conducted to verify

TABLE 1. Dehazing quantitative evaluations result in terms of average PSNR (dB) and SSIM in the dataset of [17] (reb font: 1^{st}, blue font: 2^{st} and green font: 3^{st}).

500 synthetic indoor images in SOTS [17]										
	DCP [7]	BCCR [32]	GRM [33]	CAP [8]	NLD [34]	DehazeNet [12]	MSCNN [15]	AOD-Net [13]	GMAN [35]	DRHNet
PSNR	18.87	17.87	20.44	21.31	18.53	22.66	20.01	21.01	27.94	31.39
SSIM	0.794	0.770	0.823	0.824	0.702	0.833	0.791	0.837	0.897	0.974
500 synthetic outdoor images in SOTS [17]										
	DCP [7]	BCCR [32]	GRM [33]	CAP [8]	NLD [34]	DehazeNet [12]	MSCNN [15]	AOD-Net [13]	GMAN [35]	DRHNet
PSNR	18.54	17.71	20.77	23.95	19.52	26.84	21.73	24.08	28.58	30.23
SSIM	0.710	0.741	0.762	0.869	0.733	0.826	0.831	0.873	0.909	0.973
10 synthetic images in HSTS [17]										
	DCP [7]	BCCR [32]	GRM [33]	CAP [8]	NLD [34]	DehazeNet [12]	MSCNN [15]	AOD-Net [13]	GMAN [35]	DRHNet
PSNR	17.27	16.61	20.48	22.88	18.92	26.94	20.53	23.41	20.24	29.79
SSIM	0.721	0.695	0.763	0.822	0.741	0.876	0.789	0.862	0.793	0.942

the superiority of the proposed DRHNet. Through the experimental results on synthetic datasets and real-world datasets, we can conclude that the proposed DRHNet can achieve state-of-the-art dehaziing performance.

1) QUANTITATIVE EVALUATION FOR SYNTHETIC IMAGES

As shown in Table 1, we compare the proposed DRHNet with several state-of-the-art image dehazing algorithms quantitatively, including two representative traditional algorithms, i.e., Dark-Channel Prior (DCP) [7] and Boundary Constrained Context Regularization (BCCR) [32], and three latest traditional image dehazing algorithms, i.e., Gradient Residual Minimization (GRM) [33], Color Attenuation Prior (CAP) [8], Non-local Image Dehazing (NLD) [34], and four learning-based methods, i.e., DehazeNet [12], Multi-scale CNN (MSCNN) [15], All-in-One Dehazing Network (AOD-Net) [13] and Generic model-agnostic convolutional neural network (GMAN) [35]. The quantitative evaluation was performed on the three testing sets, which include 500 synthetic indoor images in SOTS [17], 500 synthetic outdoor images in SOTS [17], and 10 synthetic images in (HSTS) [17]. We evaluate these algorithms using two full-reference image quality assessment measures: the Peak Signal to Noise Ratio (PSNR) and the Structure Similarity (SSIM) [37]. Table 1 shows the PSNR and SSIM scores of the comparison algorithms and the proposed DRHNet on three different testing sets. As shown in Table 1, we can see that the proposed DRHNet outperforms the other state-of-the-art dehazing algorithms by a large margin.

2) QUALITATIVE EVALUATION FOR SYNTHETIC IMAGES

Fig. 6 shows the dehazed images obtained from different image dehazing algorithms in the synthetic datasets. As shown in Fig. 6, we can observe that the DCP [7], GRM [33], and CAP [8] overestimate the haze thickness, so the dehazed results tend to darker than the ground truth, especially the building region of the fifth image of Fig. 6(b), Fig. 6(c) and Fig. 6(d). The dehazed results of DehazeNet [12] and AOD-Net [13] are shown in Fig. 6(e) - 6(f). Although the dehazed results by DehazeNet and AOD-Net are similar to the ground truth (GT) than the dehazed results by DCP [7], GRM [33], and CAP [8], there is still some remaining haze in the dehazed results, especially the sixth image of Fig. 6(e) and Fig. 6(f). The dehazed results generated by GMAN [35] and the proposed DRHNet are most similar to the GT. But the quantitative evaluation score of DRHNet is higher than GMAN [35]. Therefore, the performance of DRHNet is better than GMAN [35].

3) QUANTITATIVE EVALUATION FOR REAL-WORLD IMAGES

To further evaluate the dehazed performance of the proposed DRHNet and other image dehazing algorithms in the real-world hazy images, we collected the 30 real-world hazy images for evaluating. As the ground truth of the real-world image is not available, we can not evaluate the dehazed performance on real-world datasets by full-reference image quality assessment measures, i.e., PSNR and SSIM. Therefore, we compare the proposed DRHNet with different dehazing algorithms using reduced-reference and no-reference image quality assessment, i.e., spatial-spectral entropy-based quality (SSEQ) [38] and the rate of new visible edges (e) [39]. Table 2 exhibits the result of the proposed DRHNet and other state-of-the-art dehazing algorithms on the collected real-world dataset. From Table 2, we can observe that the proposed DRHNet outperforms the current state-of-the-art methods. Therefore, we can conclude that the proposed DRHNet can achieve excellent performance on real-world hazy images.

4) QUALITATIVE EVALUATION FOR REAL-WORLD IMAGES

As most of the state-of-the-art dehazing algorithms can obtain acceptable results on real-world images, it is challenging to rank them perceptibly. To compare the proposed DRHNet with other state-of-the-art dehazing algorithms, we focus on six representative images from the dataset of Ref. [7]. Fig. 7 shows a qualitative comparison with six advanced dehazing algorithms on these six challenging images. As shown

TABLE 2. Dehazing quantitative evaluations result in terms of average SSEQ and e in the real-word dataset (reb font: 1^{st}, blue font: 2^{st} and green font: 3^{st}).

Average no-reference evaluations result of dehazed results on 30 challenging real-word images.										
	DCP [7]	BCCR [32]	GRM [33]	CAP [8]	NLD [34]	DehazeNet [12]	MSCNN [15]	AOD-Net [13]	GMAN [35]	DRHNet
SSEQ	21.27	22.50	23.14	21.46	21.46	21.27	21.48	20.10	23.66	24.31
e	0.72	0.76	0.60	0.64	0.65	0.56	0.54	0.59	0.64	0.77

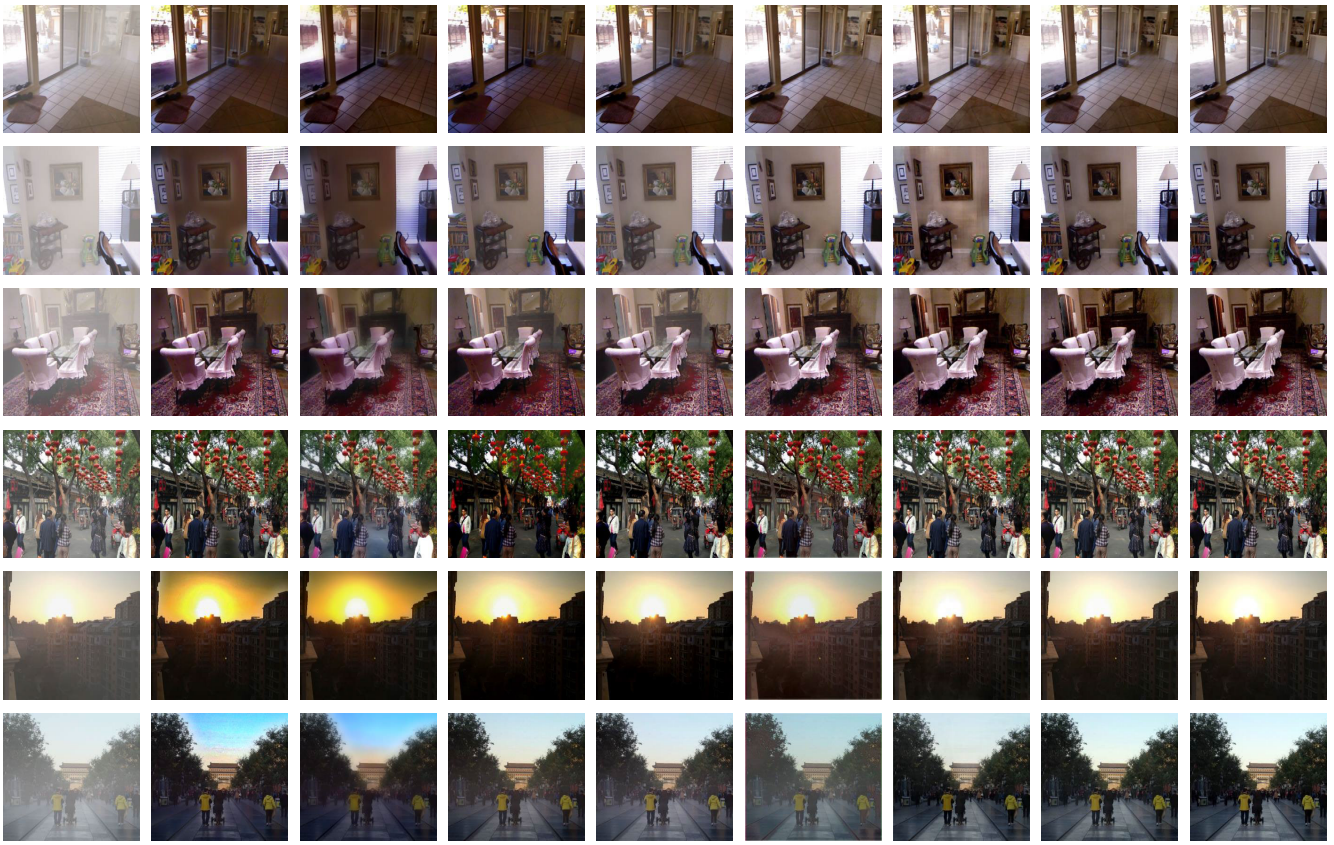

FIGURE 6. The dehazing effect of different image dehazing algorithms on synthetic images [17].

in Fig. 7, the dehazed results by DCP [7] also achieve decent dehazed performance. However, the dehazed images still suffered by color distortions. For example, the color of the dehazed *Tiananmen* image by DCP [7] is different from that in the real scene. GRM [33] achieved excellent dehazed performance on *Gugong*, but other dehazed results are not visually pleasing. Similar to DCP, CAP [8] tends to overestimate the thickness of the haze, which causes the dehazed results darker than the real scene. For example, the color of the dehazed *Gugong* image tends to be darker than the actual color, especially in the white region. DehazeNet [12] can enhance image visibility and clearness, but the dehazed result on *Canyon* is still blurry. The dehazed results of AOD-Net on *Tiananmen*, *Forest*, and *Canyon* tend to underestimate the haze thickness, which causes some remaining haze. GMAN can enhance the image visibility and augment the image details on the real-world images, excluding the image of *Canyon*. In general, the dehazed results obtained by the proposed DRHNet on real-world hazy images are visually more pleasing.

C. QUANTITATIVE AND QUALITATIVE EVALUATION FOR IMAGE DERAINING

We adopt the representative dataset [36] for training and testing to demonstrate the superiority of the proposed DRHNet on the image deraining task. We compare the proposed DRHNet with other state-of-the-art image deraining algorithms, i.e., Discriminative sparse coding-based method (DSC) [40], Gaussian mixture model (GMM) [41], CNN Method (CNN) [42], Joint Rain Detection and Removal (JORDER) [43], Deep detailed Network method (DDN) [44], Joint Bi-layer (JBO) [45], De-raining method using

(a) Hazy image (b) DCP [7] (c) GRM [33] (d) CAP [8] (e) DehazeNet [12] (f) AOD-Net [13] (g) GMAN [35] (h) DRHNet

FIGURE 7. The dehazing effect of different image dehazing algorithms on real-world images. (From the first image to the sixth image, they are New York, Hong Kong, Tiananmen, Forest, Canyon, Gugong, respectively.)

TABLE 3. Deraining quantitative results evaluated in terms of average PSNR (dB) and SSIM in the dataset of [36] (reb font: 1^{st}, blue font: 2^{st} and green font: 3^{st}).

	Input	DSC [40]	GMM [41]	CNN [42]	JORDER [43]	DDN [44]	JBO [45]	DID-MIN [36]	UMRL [46]	DRHNet
PSNR	21.15	21.44	22.75	22.07	24.32	27.33	23.05	27.95	29.77	31.58
SSIM	0.7781	0.7896	0.8352	0.8422	0.8622	0.8978	0.8522	0.9087	0.920	0.9352

a Multi-stream Dense Network (DID-MDN) [36] and Uncertainty guided Multi-scale Residual Learning using cycle spinning (UMRL) [46]. The quantitative and qualitative evaluation for image deraining is presented in Table 3 and Fig. 8. As shown in Table 3, our DRHNet achieves best performances in both PNSR and SSIM values on this synthetic dataset and significantly improves the latest UMRL [46] 1.81 dB in PSNR. As shown in Fig. 8, the proposed DRHNet has achieved excellent image deraining performance.

D. PERFORMANCE ON WHITE SCENERY IMAGES

To the best of our knowledge, image dehazing algorithms often fail in white scenes or objects. Many useful dehazing algorithms, such as the DCP [7] and CAP [8], fail on white scenes and the DehazeNet [12] relies on the robustness of white regions, but this causes the inevitable sacrifices of the visual details. Although the DRHNet does not consider or design particular parts to handle white scenes, our algorithm seems to have stronger robustness. Fig. 9 exhibits two images of white objects and their dehazed results obtained by the representative dehazing algorithms. The unbearable shadows of the DCP [7] results are easily observed, especially in the marked regions of the first row. This problem is alleviated in the GRM [33], CAP [8], DehazeNet [12] and AOD-Net [13], but still persists. However, the proposed DRHNet has stronger robustness in white scenery images, even in the challenging regions of the cat's mouth and swan's neck, DRHNet does not introduce fake color or lose original details.

E. PERFORMANCE ON HAZE-FREE IMAGES

Although the DRHNet is trained on hazy images, it has limited negative impacts on haze-free images. This is a highly desirable property as it demonstrates the effectiveness and

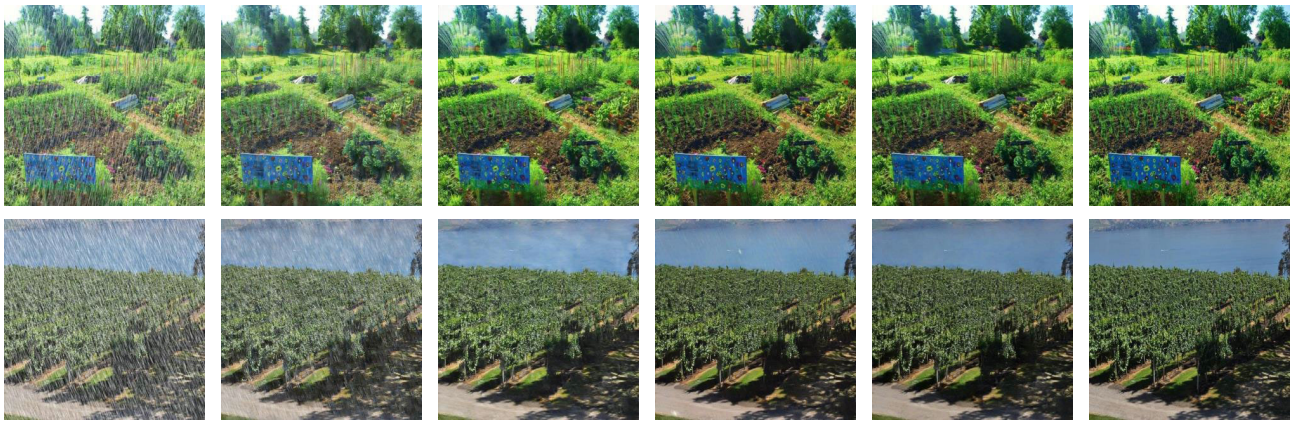

FIGURE 8. Image deraining results on sample images from the synthetic dataset [36].

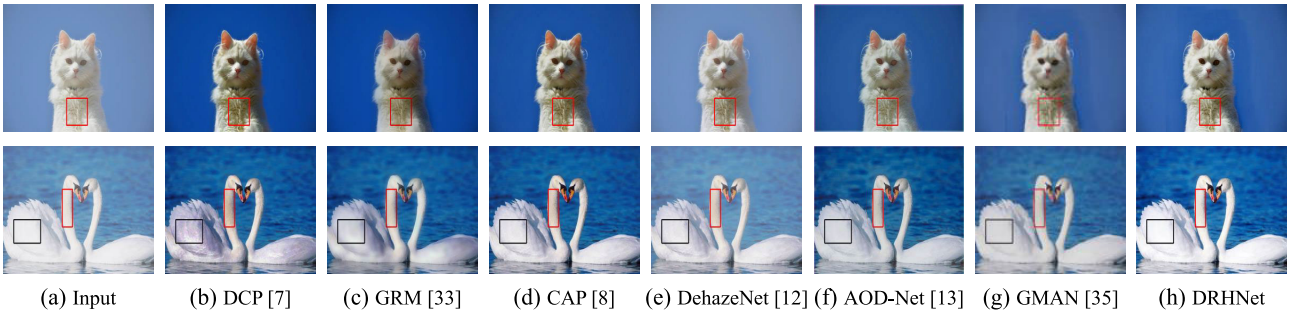

FIGURE 9. White scenery image dehazing result.

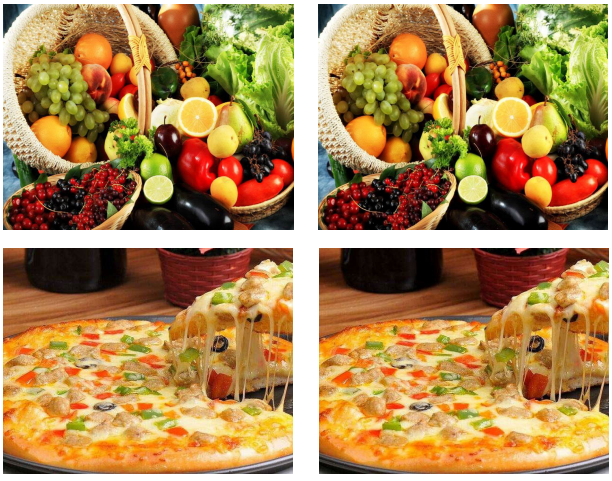

FIGURE 10. Examples of impacts over haze-free images. Left column: haze-free images. Right column: outputs by DRHNet.

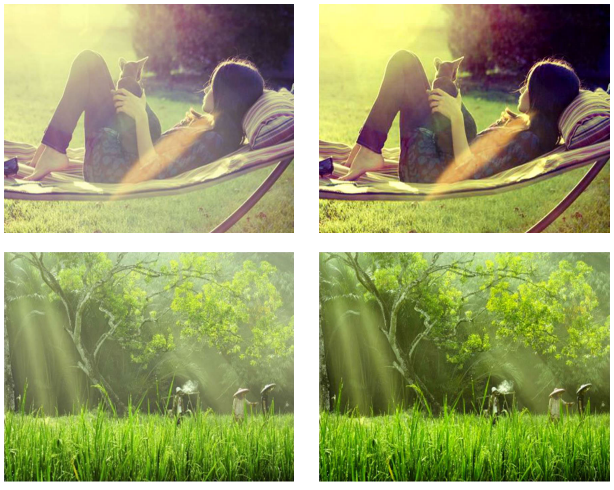

FIGURE 11. Image enhancement for anti-halation by DRHNet. Left column: real photos with halation. Right column: results by DRHNet.

robustness of the DRHNet. Fig. 10 shows the output results of two challenging haze-free images by the proposed DRHNet.

F. IMAGE ANTI-HALATION PERFORMANCE

Halation is the spreading of light beyond appropriate boundaries and forms an undesirable haze effect in image bright areas [13]. Due to the color offset caused by haze particles and light sources, the color of halation is sometimes similar to haze. We applied the DRHNet to anti-halation task without retraining to verify its robustness to these situations. As shown in Fig. 11), the results of the anti-halation by DRHNet are also excellent.

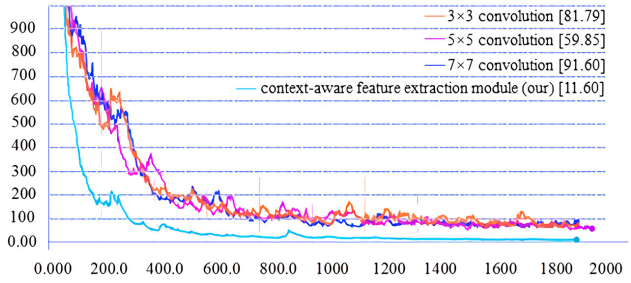

(a) The training process with different feature extraction models in first layer.

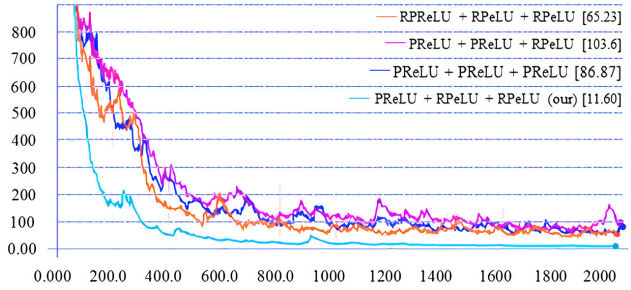

(b) The training process with different activation functions in DRHNet.

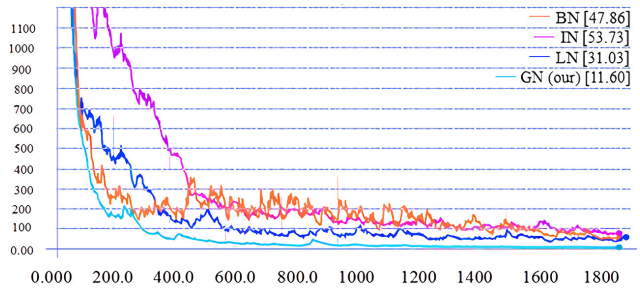

(c) The training process with different normalization methods.

FIGURE 12. Detailed abalation analysis for each important components with different configurations.

G. MODEL AND PERFORMANCE

We have conducted a series of ablation experiments to verify the performance of each specific design or choice for DRHNet. Specifically, we focus on three major components, including the context-aware feature extraction module / comment convolution, RPReLU / PReLU, GN / other normalization methods. In addition, the influence of the transformation component layers on the performance and running speed is also analyzed.

1) DIFFERENT FEATURE EXTRACTION MODELS IN THE FIRST LAYER

The context-aware feature extraction module is designed to extract multi-scale haze-relevant features. We conducted a series of experiments to prove the proposed context-aware feature extraction module can effectively improve the performance of the DRHNet. Fig. 12(a) shows the learning process when different convolution is used in the first layer of the proposed DRHNet. We can observe that the convergence speed of the context-aware feature extraction module is faster than the convergence speef when other common convolutions are used, and the loss value is 70.19, 48.25, 80.00 lower than that when 3×3, 5×5 and 7×7 convolutions are used, respectively. Therefore, the proposed context-aware feature extraction module can improve the performance of the DRHNet in the image dehazing task.

2) COMBINATION OF DIFFERENT ACTIVATION FUNCTIONS IN DRHNeT

The RPReLU is a novel activation function with certain advantages in image dehazing because it is based on some prior knowledge of hazy images. In this ablation experiment, the PReLU is used to gradually replace the RPReLU in the context-aware encoder, transformation, and haze decoder. The selected activation function in each part is illustrated in the upper right corner of Fig. 12(b). The first item represents the activation function used in the context-aware encoder component, the second item represents the activation function used in the transformation component, and the third item represents the activation function used in the haze decoder component. The experimental results prove that the proposed DRHNet has the best performance when PReLU is used in a context-aware encoder component, and RPReLU is used in the transformation component and haze decoder component.

3) DIFFERENT NORMALIZATION METHODS FOR DRHNeT

To investigate the most suitable normalization method, we adopt four different normalization methods to conduct experiments, respectively. The normalization methods used in the experiments have GN (which is selected by us) as well as BN, IN, and LN. As shown in Fig. 12(c), GN is most suitable for the proposed DRHNet.

4) DIFFERENT TRANSFORMATION IN DRHNeT

The performance would improve with the increase of layers in the network when the bottleneck building blocks were used to extract high-level features [16]. However, in most of the computer vision applications, it is desired to obtain the best trade-off between dehazing performance and parameter size. To get the best trade-off between dehazing performance and parameter size, we gradually supplement the bottleneck building blocks in the transformation component. As shown in Table. 4, we experimented with four network structures with different transformation components. Table. 4 shows the training loss and test loss for different structures.

Overall, the DRHNet with ten bottleneck building blocks had the best performance, but its training loss and testing loss were higher than other structures. The losses of DRHNet with seven bottleneck building blocks were also small (11.60/12.73) compared to the DRHNet with ten bottleneck building blocks (11.33/12.72). As far as we know, choosing a reasonable structure to balance the performance and losses is more important than only achieving the best performance. Therefore, as shown in Table. 4, the seven-layer

TABLE 4. Comparison on transformation component part in different layers.

Architecture	Training losses	Testing losses	# Param
1 layer	29.63	33.44	29,566,558
3 layers	22.97	27.07	32,982,632
7 layers	11.60	12.73	39,814,782
10 layers	11.33	12.72	44,938,895

transformation component is the best choice for the proposed DRHNet.

V. CONCLUSION

In this paper, we proposed a novel end-to-end deep residual haze network termed as DRHNet for single image dehazing and deraining. DRHNet designed a context-aware feature extraction module to aggregate the contextual information more effectively and proposed a novel activation function called RPReLU to accelerate the convergence of DRHNet. Experiments on RESIDE [17] demonstrated the superiority of DRHNet over the counterparts. In addition, experiments on the image deraining dataset proposed by Zhang and Patel [36] also demonstrated its significant improvement of performance on image deraining. In the future, we are interested in the researches on general deep learning networks for a variety of image restoration tasks, or on extension of the network for video dehazing task.

REFERENCES

[1] C. Tian, Y. Xu, and W. Zuo, "Image denoising using deep CNN with batch renormalization," *Neural Netw.*, vol. 121, pp. 461–473, Jan. 2020.

[2] J. Ker, L. Wang, J. Rao, and T. Lim, "Deep learning applications in medical image analysis," *IEEE Access*, vol. 6, pp. 9375–9389, 2018.

[3] J. Zhang, B. Chen, M. Zhou, H. Lan, and F. Gao, "Photoacoustic image classification and segmentation of breast cancer: A feasibility study," *IEEE Access*, vol. 7, pp. 5457–5466, 2019.

[4] C. Zhou, H. Fan, and Z. Li, "Tonguenet: Accurate localization and segmentation for tongue images using deep neural networks," *IEEE Access*, vol. 7, pp. 148779–148789, 2019.

[5] Z. Li, G. Liu, D. Zhang, and Y. Xu, "Robust single-object image segmentation based on salient transition region," *Pattern Recognit.*, vol. 52, pp. 317–331, Apr. 2016.

[6] H. Fan, F. Zhang, L. Xi, Z. Li, G. Liu, and Y. Xu, "LeukocyteMask: An automated localization and segmentation method for leukocyte in blood smear images using deep neural networks," *J. Biophotonics*, vol. 12, no. 7, 2019, Art. no. e201800488.

[7] K. He, J. Sun, and X. Tang, "Single image haze removal using dark channel prior," *IEEE Trans. Pattern Anal. Mach. Intell.*, vol. 33, no. 12, pp. 2341–2353, Dec. 2011.

[8] Q. Zhu, J. Mai, and L. Shao, "A fast single image haze removal algorithm using color attenuation prior," *IEEE Trans. Image Process.*, vol. 24, no. 11, pp. 3522–3533, Nov. 2015.

[9] E. J. McCartney, "Optics of the atmosphere: Scattering by molecules and particles," *Phys. Bull.*, vol. 28, no. 11, pp. 521–531, 1977.

[10] S. K. Nayar and S. G. Narasimhan, "Vision in bad weather," in *Proc. 7th IEEE Int. Conf. Comput. Vis.*, vol. 2, Sep. 1999, pp. 820–827.

[11] S. Narasimhan and S. Nayar, "Contrast restoration of weather degraded images," *IEEE Trans. Pattern Anal. Mach. Intell.*, vol. 25, no. 6, pp. 713–724, Jun. 2003.

[12] B. Cai, X. Xu, K. Jia, C. Qing, and D. Tao, "DehazeNet: An end-to-end system for single image haze removal," *IEEE Trans. Image Process.*, vol. 25, no. 11, pp. 5187–5198, Nov. 2016.

[13] B. Li, X. Peng, Z. Wang, J. Xu, and D. Feng, "AOD-Net: All-in-one dehazing network," in *Proc. IEEE Int. Conf. Comput. Vis.*, Oct. 2017, pp. 4770–4778.

[14] D. Yang and J. Sun, "Proximal dehaze-net: A prior learning-based deep network for single image dehazing," in *Proc. Eur. Conf. Comput. Vis. (ECCV)*, 2018, pp. 702–717.

[15] W. Ren, S. Liu, H. Zhang, J. Pan, X. Cao, and M.-H. Yang, "Single image dehazing via multi-scale convolutional neural networks," in *Proc. Eur. Conf. Comput. Vis.*, 2016, pp. 154–169.

[16] K. He, X. Zhang, S. Ren, and J. Sun, "Deep residual learning for image recognition," in *Proc. IEEE Conf. Comput. Vis. Pattern Recognit.*, Jun. 2016, pp. 770–778.

[17] B. Li, W. Ren, D. Fu, D. Tao, D. Feng, W. Zeng, and Z. Wang, "Benchmarking single image dehazing and beyond," 2017, *arXiv:1712.04143*. [Online]. Available: https://arxiv.org/abs/1712.04143

[18] R. T. Tan, "Visibility in bad weather from a single image," in *Proc. IEEE Conf. Comput. Vis. Pattern Recognit.*, Jun. 2008, pp. 1–8.

[19] C. O. Ancuti, C. Ancuti, C. Hermans, and P. Bekaert, "A fast semi-inverse approach to detect and remove the haze from a single image," in *Proc. Asian Conf. Comput. Vis.*, 2010, pp. 501–514.

[20] S. Zhang, C. Qing, X. Xu, J. Jin, and H. Qin, "Dehazing with improved heterogeneous atmosphere light estimation and a nonlinear color attenuation prior model," in *Proc. 10th Int. Symp. Commun. Syst., Netw. Digit. Signal Process. (CSNDSP)*, 2016, pp. 1–6.

[21] T. M. Bui and W. Kim, "Single image dehazing using color ellipsoid prior," *IEEE Trans. Image Process.*, vol. 27, no. 2, pp. 999–1009, Feb. 2018.

[22] S. Ting *et al.*, "Defogging algorithm based on the prior dark-channel and theory of retinex," *Natural Sci. Ed., J. Jishou Univ.*, vol. 35, pp. 12–20, 2014.

[23] L. Huang, "The algorithm of segmenting the prior neighborhood of dark channel in the single image dehazing," *J. Jishou Univ.*, vol. 20, no. 2, pp. 228–234, 2018.

[24] Y. Wu and K. He, "Group normalization," in *Proc. Eur. Conf. Comput. Vis. (ECCV)*, 2018, pp. 3–19.

[25] S. Ioffe and C. Szegedy, "Batch normalization: Accelerating deep network training by reducing internal covariate shift," 2019, *arXiv:1502.03167*. [Online]. Available: https://arxiv.org/abs/1502.03167

[26] D. Ulyanov and A. Vedaldi, "Instance normalization: The missing ingredient for fast stylization," 2016, *arXiv:1607.08022*. [Online]. Available: https://arxiv.org/abs/1607.08022

[27] J. L. Ba, J. R. Kiros, and G. E. Hinton, "Layer normalization," 2016, *arXiv:1607.06450*. [Online]. Available: https://arxiv.org/abs/1607.06450

[28] K. He, X. Zhang, S. Ren, and J. Sun, "Delving deep into rectifiers: Surpassing human-level performance on imagenet classification," in *Proc. IEEE Int. Conf. Comput. Vis.*, Dec. 2015, pp. 1026–1034.

[29] H. Zhang and V. M. Patel, "Densely connected pyramid dehazing network," in *Proc. IEEE Conf. Comput. Vis. Pattern Recognit.*, Jun. 2018, pp. 3194–3203.

[30] J. Johnson, A. Alahi, and F. Li, "Perceptual losses for real-time style transfer and super-resolution," in *Proc. Eur. Conf. Comput. Vis.*, 2016, pp. 694–711.

[31] K. Simonyan and A. Zisserman, "Very deep convolutional networks for large-scale image recognition," in *Proc. Int. Conf. Learn. Represent.*, 2015.

[32] G. Meng, Y. Wang, J. Duan, S. Xiang, and C. Pan, "Efficient image dehazing with boundary constraint and contextual regularization," in *Proc. IEEE Int. Conf. Comput. Vis.*, Dec. 2013, pp. 617–624.

[33] C. Chen, N. Do, and J. Wang, "Robust image and video dehazing with visual artifact suppression via gradient residual minimization," in *Proc. Eur. Conf. Comput. Vis.*, 2016, pp. 576–591.

[34] D. Berman and S. Avidan, "Non-local image dehazing," in *Proc. IEEE Conf. Comput. Vis. Pattern Recognit.*, Jun. 2016, pp. 1674–1682.

[35] Z. Liu, B. Xiao, M. Alrabeiah, K. Wang, and J. Chen, "Single image dehazing with a generic model-agnostic convolutional neural network," *IEEE Signal Process. Lett.*, vol. 26, no. 6, pp. 833–837, Jun. 2019.

[36] H. Zhang and V. M. Patel, "Density-aware single image de-raining using a multi-stream dense network," in *Proc. IEEE Conf. Comput. Vis. Pattern Recognit.*, Jun. 2018, pp. 695–704.

[37] Z. Wang, A. Bovik, H. Sheikh, and E. Simoncelli, "Image quality assessment: From error visibility to structural similarity," *IEEE Trans. Image Process.*, vol. 13, no. 4, pp. 600–612, Apr. 2004.

[38] L. Liu, B. Liu, H. Huang, and A. C. Bovik, "No-reference image quality assessment based on spatial and spectral entropies," *Signal Process., Image Commun.*, vol. 29, no. 8, pp. 856–863, 2014.

[39] N. Hautiére, J.-P. Tarel, D. Aubert, and É. Dumont, "Blind contrast enhancement assessment by gradient ratioing at visible edges," *Image Anal. Stereol.*, vol. 27, no. 2, pp. 87–95, Jul. 2008.
[40] Y. Luo, Y. Xu, and H. Ji, "Removing rain from a single image via discriminative sparse coding," in *Proc. IEEE Int. Conf. Comput. Vis.*, Dec. 2015, pp. 3397–3405.
[41] Y. Li, R. Tan, X. Guo, J. Lu, and M. S. Brown, "Rain streak removal using layer priors," in *Proc. IEEE Conf. Comput. Vis. Pattern Recognit.*, Jun. 2016, pp. 2736–2744.
[42] X. Fu, J. Huang, X. Ding, Y. Liao, and J. Paisley, "Clearing the skies: A deep network architecture for single-image rain removal," *IEEE Trans. Image Process.*, vol. 26, no. 6, pp. 2944–2956, Jun. 2017.
[43] W. Yang, R. T. Tan, J. Feng, J. Liu, Z. Guo, and S. Yan, "Deep joint rain detection and removal from a single image," in *Proc. IEEE Conf. Comput. Vis. Pattern Recognit. (CVPR)*, Jul. 2017, pp. 1357–1366.
[44] X. Fu, J. Huang, D. Zeng, Y. Huang, X. Ding, and J. Paisley, "Removing rain from single images via a deep detail network," in *Proc. IEEE Conf. Comput. Vis. Pattern Recognit.*, Jul. 2017, pp. 1715–1723.
[45] L. Zhu, C. Fu, D. Lischinski, and P.-A. Heng, "Joint bi-layer optimization for single-image rain streak removal," in *Proc. IEEE Int. Conf. Comput. Vis.*, Oct. 2017, pp. 2526–2534.
[46] R. Yasarla and V. M. Patel, "Uncertainty guided multi-scale residual learning-using a cycle spinning CNN for single image de-raining," in *Proc. IEEE Conf. Comput. Vis. Pattern Recognit.*, Jun. 2019, pp. 8405–8414.

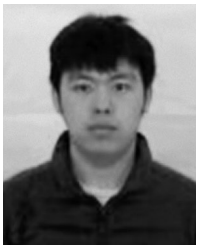

CHUANSHENG WANG is currently pursuing the M.S. degree with the School of Computer Science and Technology, Harbin University of Science and Technology, Harbin, China. His current research interests include pattern recognition, machine learning, and digital signal process.

ZUOYONG LI received the B.S. and M.S. degrees in computer science and technology from Fuzhou University, Fuzhou, China, in 2002 and 2006, respectively, and the Ph.D. degree from the School of Computer Science and Technology, Nanjing University of Science and Technology (NUST), Nanjing, China, in 2010. He is currently a Professor with the College of Computer and Control Engineering, Minjiang University, Fuzhou, China. He has published over 60 articles in international/national journals. His current research interests are image processing, pattern recognition, and machine learning.

JIAWEI WU is currently pursuing the B.E. degree with the College of Computer and Control Engineering, Minjiang University, Fuzhou, China. His current research interests include computer vision and deep learning.

HAOYI FAN received the B.E. degree from the School of Mathematics, Zhengzhou University of Aeronautics, Zhengzhou, China, in 2015. He is currently pursuing the Ph.D. degree with the School of Computer Science and Technology, Harbin University of Science and Technology, Harbin, China. His current research interests include pattern recognition, information security, and machine learning.

GUOBAO XIAO received the Ph.D. degree in computer science and technology from Xiamen University, China, in 2016. He was a Postdoctoral Fellow with the School of Aerospace Engineering, Xiamen University, from 2016 to 2018. He is currently a Professor with Minjiang University, China. He has published more than 30 articles in international journals and conferences, including the IEEE TRANSACTIONS ON PATTERN ANALYSIS AND MACHINE INTELLIGENCE, the *International Journal of Computer Vision*, *Pattern Recognition Letters*, *Computer Vision and Image Understanding*, ICCV, ECCV, ACCV, AAAI, ICIP, and ICARCV. His research interests include machine learning, computer vision, pattern recognition, and bioinformatics. He received the Best Ph.D. Thesis in Fujian Province and the Best Ph.D. Thesis Award from the China Society of Image and Graphics. He serves on the reviewer panel for some international journals and top conferences.

HONG ZHANG received the B.E., M.Sc., and Ph.D. degrees from the Harbin Institute of Technology (HIT), in 1984, 1984, and 2007, respectively. His research interests include digital signal process, testing instrument, and embedded systems.